Article

Hybrid Perovskite/Polymer Materials: Preparation and Physicochemical Properties

Martha Kafetzi, Stergios Pispas * and **George Mousdis ***

Theoretical and Physical Chemistry Institute, National Hellenic Research Foundation, 48 Vassileos Constantinou Avenue, 11635 Athens, Greece; mkafetzi91@gmail.com
* Correspondence: pispas@eie.gr (S.P.); mousdis@eie.gr (G.M.); Tel.: +30-210-727-3824 (S.P.); +30-210-727-3838 (G.M.)

Abstract: The aim of this work is to investigate the preparation, the optical properties, and the stability over time of a colloidal organic–inorganic hybrid perovskite ($CH_3NH_3PbBr_3$)/random copolymer P(MMA-co-DMAEMA) system. Different ratios of perovskite to copolymer were used to study its effect on stability and properties. The optical properties were investigated by UV-Vis and fluorescence spectroscopy. Dynamic light scattering was used to determine the size, and the size polydispersity of the colloidal hybrid particles; while morphology was investigated by transmission electron microscopy. Photoluminescence decay studies revealed the interaction of the random copolymer with the perovskite. Finally, thin-films were prepared, to investigate the optical properties of the samples in the absence of the solvent. High temporal stability of the optical properties of thin hybrid films was observed under certain conditions.

1. Introduction

Organic–inorganic hybrid perovskites (Hyb-Per) are an emerging class of solution processable semiconducting materials that combine the favorable properties of the inorganic semiconductor with the flexibility and low-temperature process ability of the organic material [1,2]. They show excellent optoelectronic properties, such as a high and balanced carrier mobility [3,4], long carrier diffusion length [5], tunable bandgap [6], high photoluminescence quantum yield, and large light absorption coefficient in the UV–Vis range [7,8]. By choosing the appropriate amine-metal-halogen combination, the optical band gap, as well as their emission and absorption spectra, can be controlled throughout the entire visible range [9–11]. The Hyb-Per can be prepared with quick and easy synthetic procedures and their thin-films can be produced easily even on an industrial scale, using low-cost film-deposition techniques that allow the adjustment in morphology, composition, and crystalline properties. Because of their easy and quick synthesis procedures and their optical and semiconducting properties, Hyb-Per have already shown a tremendous potential for use in optoelectronic devices [12] such as light-emitting diodes (LEDs) [13], photodetectors [14], lasers [15], and field-effect transistors (FETs) [16]. Especially, their use for photovoltaic applications took the photovoltaic community by storm with an improvement of the solar to electric conversion efficiency from 3.8 to 22.1% in just six years [17].

Lately, the expanded use of LEDs for artificial lighting and imaging, due to better quality and significant energy savings, increase the effort for the preparation of new materials to replace the expensive inorganic semiconductors prepared with vacuum-based epitaxial growth on expensive rigid substrates. The high photoluminescence quantum yield, narrow full width to half-maximum (≈20 nm) [18], and the easiness of Hyb-Per synthesis and their film preparation has placed them among the strong candidates as materials for light-emitting diode (PLED) devices and display applications [13].

The crystal structure of (CH3NH3)PbX3, (X: Cl, Br, I) consists of two different components, an inorganic network of corner sharing PbX6 octahedra and organic cations (CH3NH$_3$$^+$) in the voids of the network. By mixing and grinding the precursor salts at room temperature, nanocrystals of the organic–inorganic hybrid perovskites are formed, characteristic of the easiness with which the organic cations can diffuse into the inorganic framework. However, the size and quality of the nanocrystals prepared by this method is suffering from repeatability, due to the lack of precise control of experimental conditions. The most common synthetic route for the formation of hybrid perovskite nanocrystals is the ligand-assisted reprecipitation method. Factors such as the size and the dimensionality of nanocrystals can be adjusted by changing the synthetic procedure resulting in different optical features [19,20]. The possibility of stable hybrid perovskite nanocrystals dispersed in solution or in a polymer matrix would enable the preparation of new optoelectronic devices [21]. The preparation of Hyb-Per in the form of colloidal nanocrystals solutions is of great scientific and technological interest [22]. One of the main issues that remain to be solved is their instability towards air, temperature, light irradiation, and water. According to the ligand-assisted reprecipitation method, the inorganic metal and ammonium, halide salts were dissolved in a polar solvent and injected into a nonpolar solvent, resulting in an instantaneous formation of nanocrystals. The presence of a good capping agent is necessary to stabilize the newly formed nanocrystals. Lately, few attempts have been made to stabilize them, using amines [23], oleic acid [24], or polymers [25] as protective agents. These protected colloidal nanocrystals present increased stability over time enhanced exciton stability and many times greater photoluminescence than the bulk material [25], also the wavelength of the excitonic absorption and photoluminescence can be tailored by controlling the size of the nanoparticles [9,26].

Amphiphilic copolymers have been used extensively due to their self-assembling behavior into nanoparticles when inserted in a selective solvent [27,28]. Different architectures such as random, diblock, multiblock, star, and graft copolymers can be made by regulating the synthesis procedures [29]. The copolymer architecture and the suitability of the solvent determine the nanostructure morphology. For example, block copolymers form well-controlled and organized nanoparticles, while random copolymers form more unusual and irregular morphologies [30–32]. Hybrid, well-defined nanostructures can be accomplished by combining/mixing self-assembling of amphiphilic copolymers with inorganic, semiconducting materials. Therefore, the formed hybrid materials display improved mechanical, optical, and absorptive properties and greater stability over time [19,33,34].

Here, we report on the synthesis and investigation of the properties of a novel polymer-perovskite nanoparticles system based on CH$_3$NH$_3$PbBr$_3$ nanocrystals protected by PDMAEMA-co-PMMA copolymer. The above copolymer offers great potential as protection factor and nanocarrier because of its ability in self-assembling into organized nanostructures due to the combination of a hydrophobic/solvophobic and a hydrophilic/solvophilic part. To the best of our knowledge, it is the first time that an amphiphilic copolymer was used to protect the Hyb-Per nanocrystals. A colloidal mixture was prepared with the perovskite nanocrystals encapsulated in the polar PDMAEMA core of the hybrid assemblies. Thin hybrid films were prepared from these solutions. The colloidal solutions and the thin films were investigated by various characterization techniques.

2. Materials and Methods

2.1. Materials

The monomers MMA (99% pure) and DMAEMA (96% pure) were obtained from Alfa Aesar. 4-Methoxyphenol was used as inhibitor in both cases. For the purification of both monomers, a column filled with resins for inhibitor removal was used. 2,2′-Azobis (isobutyronitrile) (AIBN) was used as after recrystallization from methanol. 1,4-dioxane (99.8% pure), hexane (98.5% pure), tetrahydrofuran (THF, 99.9% pure), methylamine solution 40% wt. in H$_2$O, were obtained from Aldrich, lead (II) bromide (puratronic 99.9%) was obtained from Alfa.

2.2. Preparation of the Polymer-Perovskite Nanoparticles System

2.2.1. CH3NH3Br Synthesis

The CH_3NH_3Br (methylammonium bromide) was prepared as follows: 20 mL of a solution (40% w/v) containing 8 g methylamine (257 mmol) was diluted with 80 mL of ethanol. To this solution, a hydrobromic acid solution in water (57% w/v) was added slowly, under stirring, until the pH of solution turns to acidic. The solution was stirred for 2 h at room temperature and evaporated to dryness. The solid was dispersed into anhydrous diethylether and filtered. It was washed copiously with anhydrous diethylether to obtain white crystals.

### 2.2.2. P(MMA-co-DMAEMA) Random Copolymer Synthesis

P(MMA-co-DMAEMA) random copolymer (Scheme 1) was synthesized via conventional free radical polymerization (CRP). Methyl methacrylate (MMA, 2.5 g) and 2-(dimethylamino) ethyl methacrylate (DMAEMA, 7.5 g) free of inhibitors, AIBN (0.5 g) and dioxane (100 mL) were added in a round flask. The mixture was degassed by nitrogen gas bubbling and then placed in an oil bath and left to polymerize at 70 °C for 24 h. After precipitation in excess of hexane and drying in vacuum oven for 48 h, the PDMAEMA-co-MMA random copolymer was obtained in dry state. The molecular weight (Mw) was 85.000 g/mol and the polydispersity index (Mw/Mn) 1.4, both values were determined with size exclusion chromatography (SEC). The weight composition of PMMA is 77% and of PDMAEMA is 23%. The composition was calculated by the obtained ^{1}H NMR spectra.
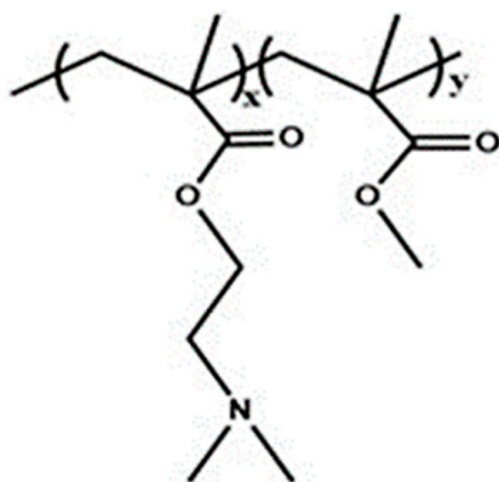
Scheme 1. Chemical structure of P (DMAEMA-co-MMA) random copolymer.

2.2.3. Preparation of the Colloidal Solution

Four different $CH_3NH_3PbBr_3$ yellow-colored solutions, were prepared by following the synthetic procedure shown in Scheme 2. Starting $CH_3NH_3PbBr_3$ DMF solutions: 7.0 mg (0.0625 mmole) of freshly prepared CH_3NH_3Br and 23.0 mg (0.0625 mmole) of $PbBr_2$ were dissolved in 10, 5, 2.50, and 1.25 mL, respectively, of dry DMF and stirred vigorously for two minutes. The molarities of the prepared solution are of 6.26 mM (Solution a), 12.5 mM (Solution b), 25.0 mM (Solution c), and 50.0 mM (Solution d), respectively. A total of 0.125 g of the copolymer was dissolved in 40 mL toluene (0.31% w/v). Then, 40 μL from the solutions a, b, c, d, were added in 5 mL of the copolymer solution under vigorous stirring to prepare the solutions 1a, 1b, 1c, 1d. Instantly, the color of the solutions turned yellow. The colloidal solutions were stirred at 500 rpm for 10 min. In order to confirm the colloidal stability that the addition of the polymer offers to the perovskite nanocrystals, blank solutions were prepared without the polymer addition. Specifically, 40 μL from the solutions a, b, c, d, were added into 5 mL of toluene, under vigorous stirring to produce the solutions 2a, 2b, 2c, 2d.
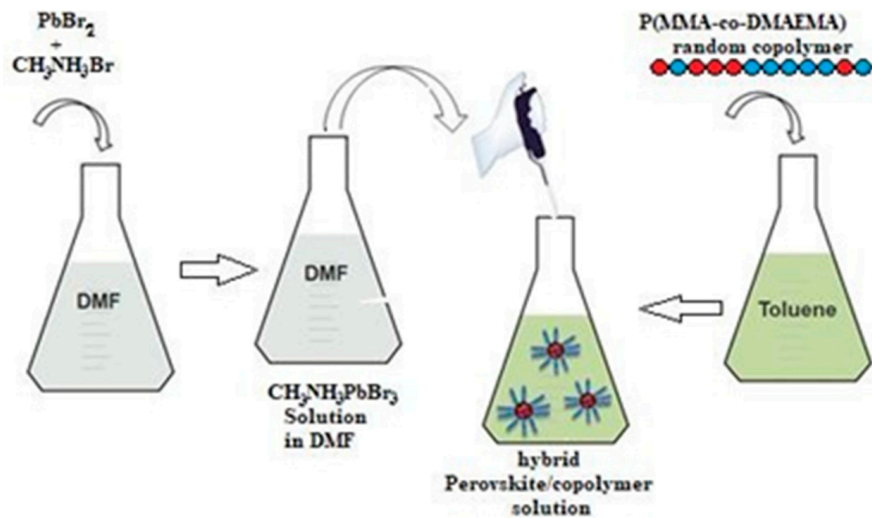
Scheme 2. Schematic illustration of the preparation of the perovskite/random copolymer hybrid material, dispersed in toluene.

2.3. Characterization

The molecular weight and the molecular weight distributions of the copolymer were calculated by size exclusion chromatography (SEC) using a Waters system. It consists of a Waters 1515 isocratic pump, a set of three μ-Styragel mixed bed columns (porosity range: 102–106 Å), a Waters 2414 refractive index detector (equilibrated at 40 °C), and Breeze software was utilized for data processing. THF, containing 5% v/v triethylamine was utilized as the mobile phase. The flow rate of the mobile phase was 1.0 mL/min at 30 °C. The instrument was calibrated by using standard polystyrene samples of narrow molecular weight distributions and average molecular weights in the range of 1200–929,000 g/mol. The measured samples were dissolved THF, at concentrations in the range of 2–4 mg/mL.

^{1}H-NMR spectra in CDCl$_3$ were gathered using a Bruker AC 300 FT-NMR spectrometer.

Mid-IR spectra in the region 550–4000 cm^{-1} were collected using a FTIR spectrometer (Equinox 55 from Bruker Optics) rigged with a single reflection diamond ATR accessory (Dura- Samp1IR II by SensIR Technologies).

Optical absorption spectra of both films and solutions were recorded on a Perkin-Elmer, Lambda 19 spectrophotometer. Steady state emission spectra were obtained by using a Jobin Yvon-Spex, Fluorolog 3 spectrophotometer with a 350 nm excitation and 2 nm slits. For the films, the front-face configuration and for the solutions, the right-angle configuration was used. Picosecond time-resolved fluorescence spectra were examined by the time correlated single photon counting (TCSPC) method on a Nano-Log spectrofluorometer (Horiba JobinYvon), by using a laser diode as an excitation source (NanoLED, 375 nm) and a UV-Vis detector TBX-PMT series (250–850 nm) by Horiba JobinYvon. Lifetimes were processed with the DAS6 Fluoroscence- Decay Analysis Software.

Dynamic light scattering measurements were carried out on an ALV/CGS-3 compact goniometer system (ALVGmbH), rigged with an ALV 5000/EPP multi-τ digital correlator with 288 channels and an ALV/LSE-5003 light scattering electronics unit for stepper motor drive and limit switch control. A JDS Uniphase 22 mW He-Ne laser (λ = 632.8 nm) was used as the light source. Toluene was used as the calibration standard. The instrument is rigged with a water bath and a thermometer for temperature variations. Autocorrelation functions were processed with the cumulants method and the CONTIN algorithm. The solutions were filtered through 0.45 μm hydrophobic TF filters (Whatman) before measurements in order to remove dust. Subsequently, standard 1 cm width quartz cells were filled with filtered samples and measurements were carried out at angles 30° to 150°.

Morphological studies of perovskite/copolymer hybrid composite structures were accomplished by using a Hitachi HT7700 Transmission Electron Microscope, operating at 100 kV. One drop of each sample dispersion was deposited on a carbon-coated grid and the

solvent was evaporated at room temperature for 24 h. After drying process was completed, the samples were studied in transmission mode.

Thin films were prepared using a Laurell WS-400BX-6NPP spin-coater. The film thickness was measured by an Alpha-Step IQ Surface Profiler.

All measurements were conducted at room temperature.

3. Results and Discussion

3.1. Hybrid Nanoparticle Preparation and Dynamic Light Scattering Measurements

P(MMA-co-DMAEMA) random copolymer was chosen as a colloidal stabilizer since the MMA segments form glassy nonpolar/hydrophobic nanodomains while the DMAEMA segments form polar/hydrophilic nanodomains in aqueous or organic solvent solutions of respective polarity. Both segments can interact with entities of similar polarity and tertiary amine groups on DMAEMA segments can also exert complexation functions towards perovskite entities.

When an amphiphilic block or random copolymer is inserted in a nonpolar medium, the hydrophilic part forms the cores of the obtained self-assembled nanoparticles while the hydrophobic part surrounds the cores. The reverse phenomenon is observed when the copolymer is inserted in a polar solvent. Thus, the copolymer matrix functions as a protective agent in order to avoid the precipitation of the crystalline $CH_3NH_3PbBr_3$ and keeps the hybrid perovskite/copolymer stable in solution. Formation of the core allows the encapsulation of the $CH_3NH_3PbBr_3$ nanocrystals, while MMA units cover the core in order to protect from precipitation and stabilize the $CH_3NH_3PbBr_3$ nanocrystals and the hybrid ensemble in nonpolar solvents. Specifically, P(MMA-co-DMAEMA) copolymers when inserted in an organic nonpolar medium such as toluene, they self-organize into nanoparticles where the DMAEMA segment forms the core and the MMA segment encompasses the polar DMAEMA segments. When the $CH_3NH_3PbBr_3$ nanocrystals are encapsulated into the DMAEMA core, intermolecular interactions develop between the DMAEMA part and the perovskite nanocrystal, while the MMA part offers colloidal stability to the system.

In order to gain information about the size, the size polydispersity, and the stability of perovskite/copolymer nanoparticles, DLS measurements were performed. The results are presented in Tables 1 and 2.

Table 1. Dynamic light scattering results for solution 1a, 1b, 1c, 1d, on the day they were prepared.

Sample	$C_{\text{perov in DMF}}$ (mM)	$C_{\text{copol in toluene}}$ (g/mL)	R_h [a] [35] (nm)
1a	6.25	3.125×10^{-3}	2.4
1b	12.5	3.125×10^{-3}	58
1c	25.0	3.125×10^{-3}	46
1d	50.0	3.125×10^{-3}	64
2a	6.25	-	N/A
2b	12.5	-	150
2c	25.0	-	123
2d	50.0	-	117

[a] Determined by DLS at measuring angle of 90°.

Table 2. Intensity and R_h values of samples 1a, 1b, 1c, 1d on 1st day, and after 7, 20, 30 days.

Day	Sample 1a		Sample 1b		Sample 1c		Sample 1d	
	Intensity [a] (kc/s)	Rh [a] [36] (nm)	Intensity [a] (kc/s)	Rh [a] [36] (nm)	Intensity [a] (kc/s)	Rh [a] [36] (nm)	Intensity [a] (kc/s)	Rh [a] [36] (nm)
1st	28	2.45	124	58	2994	45.9	18,387	64
7th	37	7.5	99	51	880	46	14,387	64
20th	34	-	53	38	612	47.2	3277	60
30th	-	-	51	53	385	46.5	2590	57

[a] Determined by DLS at measuring angle of 90°.

In all cases, a single peak from CONTIN [36], analysis of the DLS correlation functions is observed (Figure 1), indicating the homogeneity of the system in each case. Moreover, by increasing the concentration of the perovskite solution, no precipitation has occurred, suggesting that colloidal stable nanoparticles can be formed in all cases. It is observed that the nanoparticles formed, without the presence of polymer, present increased hydrodynamic radius values, relative to the corresponding ones, to which the copolymer has been added. The measurements repeated once a week for a period of one month (Figure 2). In the case of series 1, a single peak from the CONTIN analysis was observed at all times and no precipitation or significant change in the radius of the nanoparticles occurred, except for the solution 1a, which contains the lower amount of perovskite, displaying once more the stability of the system over time. The low R_h value (2.4 nm) at angle of 90 degrees as well as the low scattering intensity value (28 kc/s) of Sample 1a are attributed to the fact that the concentration value of the perovskite solution in this case is not adequate in order for mixed perovskite/random copolymer nanoparticles to be formed. Therefore, both the R_h and the scattering intensity values are due to the single chain formation of the random copolymer in toluene. According to UV-Vis spectra (Figure 3), the sample does not exhibit excitonic absorption and in combination with the low scattering light intensity, it is possible that the perovskite nanocrystals were retained on the filter. On the seventh day, an increase in the scattering light intensity value, which is accompanied with an increase in the Rh value, demonstrates the formation of nanoaggregates. Therefore, it can be assumed that the self-assembly of the random copolymer and perovskite into nanoparticles is a slow process that takes about a week long in order to be completed. On the 20th day, the intensity value has been decreased due to the precipitation of the nanoparticles. The size distribution analysis is not possible due to the presence of dust. It is possible to suppose that a certain concentration and ratio of the components is needed in order to form stable hybrid nanoparticles under the conditions utilized in this study.
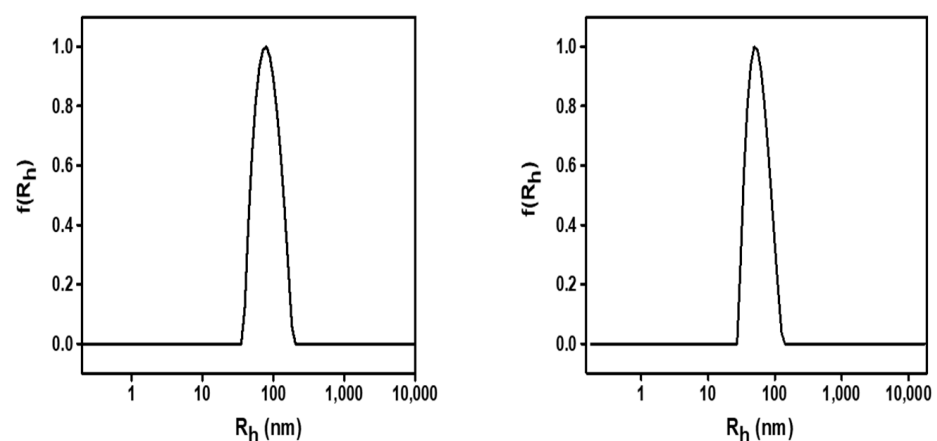

Figure 1. Size distribution from CONTIN analysis for Sample 1b (**left**) and 1d (**right**) at 90°. Data was collected on day 1.
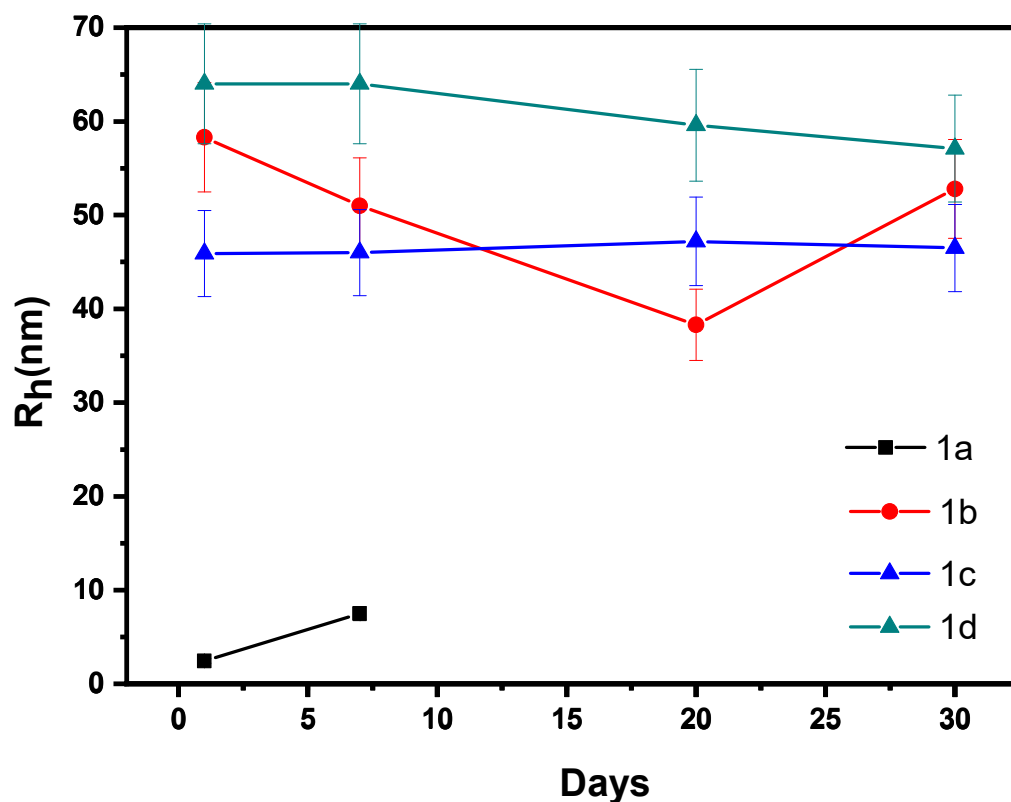
Figure 2. R_h values fluctuation for Samples 1a, 1b, 1c, and 1d from day 1 to day 30, as it was obtained from dynamic light scattering measurements.
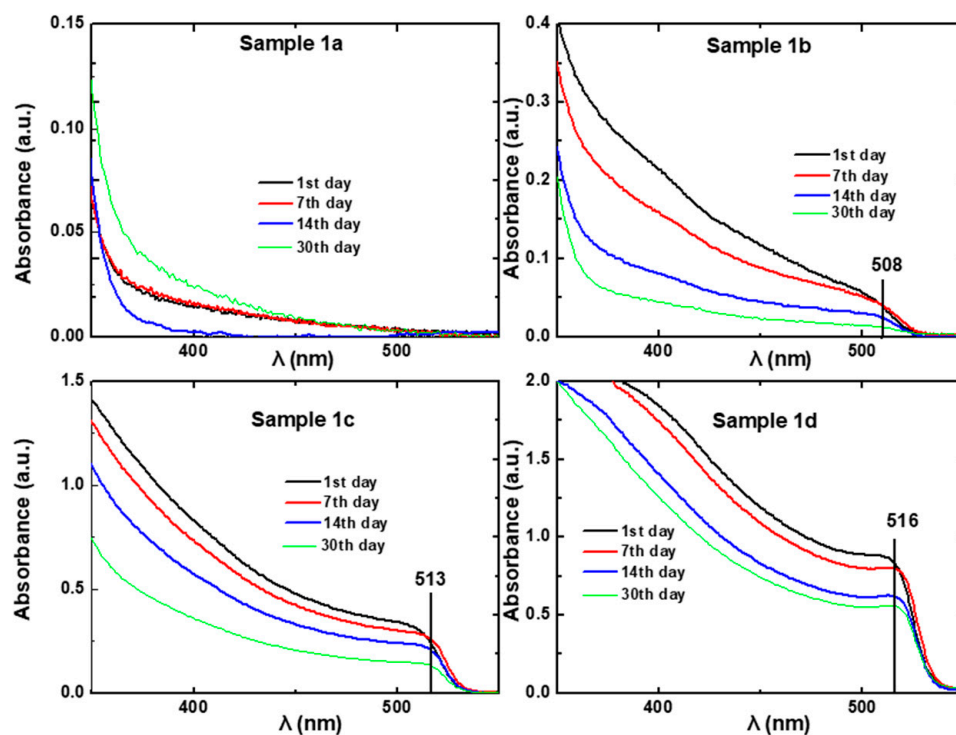

Figure 3. UV-Vis absorption spectra of solutions (1a), (1b), (1c), and (1d) from 1st (black line), 7th (red line) 14th (Blue line), and 30th (green line) day.

Concerning solution 1b, after the filtration, the solution was discolored and the larger perovskite particles were retained on the filter. We assume that certain perovskite particles were not encapsulated in the polymeric nanoparticles and this is the reason why they were retained on the filter. On the first day, the intensity and R_h values shows the presence of polydispersed nanoparticles in toluene. The perovskite nanocrystals were encapsulated in the polymeric nanoaggregates. At longer times, the intensity values decrease due possibly to particle precipitation.

No change of color was observed for solution 1c after filtration. On the first day, the intensity value was 2994 kcps (kilophotons per second) and the Rh was 46 nm. Based on the intensity value and the excitonic absorption, which is displayed in the UV-vis spectrum (Figure 3 it can be assumed that the encapsulation of the perovskite nanocrystals into the polymeric nanoparticles was successful. The 1c polymer/perovskite hybrid nanosystem exhibits high size homogeneity. At latter times, the intensity value decreases due to at least partial precipitation of the mixed polymer/perovskite nanostructures, while the hydrodynamic radius appears to be relatively stable. The high intensity value on day 7th, 20th, and 30th is due to the sufficient number of nanoparticles that are still dispersed in the solution, even though precipitation of certain nanoparticles must have occurred. Sample 1c seems to exhibit greater colloidal stability than Samples 1a and 1b, over time.

No change of color was observed also in the case of Sample 1d. This sample presents the highest size homogeneity of all. Moreover, Sample 1d exhibits the greatest intensity value of all, as high-mass mixed nanostructures are presumably formed due to the higher amount and ratio of the perovskite component in the mixed solutions. The encapsulation of perovskite nanocrystals into the polymeric nanoparticles appears to be successful. The sample appears to be stable over time, as long as the hydrodynamic radius is observed, but the scattering intensity value is partially reduced. The latter may be a sign of partial precipitation. Although a number of polymer/perovskite mixed nanoparticles precipitated, the intensity value seems to be high (but decreased compared with day 1) as there are still a large number of dispersed hybrid nanoparticles in toluene.

To sum up, for Samples 1c and 1d, formation of stable hybrid polymer/perovskite nanoparticles was observed with significant colloidal stability. The scattering light intensity is high in both cases, while Sample 1d exhibits the highest value. Both samples present great stability over time, as hydrodynamic radius measurements indicate. Specifically, Sample 1c appears to be more stable than 1d in terms of both size and intensity value. Both samples display high size homogeneity, but Sample 1d has lower polydispersity index, indicating that Sample 1d is more homogeneous than 1c. Finally, the preparation procedure was repeated several times. The results from DLS experiments were similar in all the cases, indicating the repeatability of the synthesis protocol.

For the samples prepared in the absence of copolymer (Samples 2a, 2b, 2c, 2d), formation of large nanoparticles (R_h > 100 nm) was observed, which were not stable and precipitated after some hours.

3.2. Optical Properties

3.2.1. Perovskite/Polymer Solutions

According to UV-Vis spectra (Figure 3), the sample with the lowest concentration (1a) does not exhibit excitonic absorption even from the first day. The other three samples (1b, 1c, 1d) exhibit excitonic absorption with intensities that increase as the concentration of the perovskite is increased. Moreover, a redshift is observed when the concentration of the perovskite solution is increased. Specifically, the peak of exitonic absorption of Sample 1b is observed at λ_{max} ~ 508 nm, of Sample 1c at λ_{max} ~ 513 nm and of Sample 1d at λ_{max} ~ 516 nm, indicating the formation of larger nanocrystals as the perovskite concentration increases. The exitonic peaks are slightly red shifted with the time, pointing out that the size of the nanocrystals is increased as time passes, possibly due to further reorganization phenomena. Those peaks are blue shifted compared to those of film and single crystal

$CH_3NH_3PbBr_3$ [37] (520 [38] and 550 nm [39] respectively) mainly due to the particle-size quantum confinement effect.

The sample with the lowest concentration (1a) shows a weak excitonic emission peak at 499 nm that is disappeared after some days (Figure 4). All the other samples (1b, 1c, 1d) exhibit strong excitonic emission peaks. As in the case of absorbance spectra, all the emission peaks are red shifted compared to $CH_3NH_3PbBr_3$ film and single crystal. Also, a redshift of the emission peaks is observed as the perovskite concentration gets higher, possibly due to the formation of nanocrystals of larger size. Moreover, Figure 4 suggests that photoluminescence originated from $CH_3NH_3PbBr_3$ immediately after the synthesis, which indicates that the perovskite nanocrystals have been formed. The photoluminescence intensity of Samples 1b, 1c, and 1d remain strong for the whole 30 days period of study, although there is a decrease of the intensity. The small Stokes shift of the samples indicate that the PL emission originates from direct exciton recombination. Similar spectra were obtained by $CH_3NH_3PbBr_3$ nanocrystals prepared by different methods.
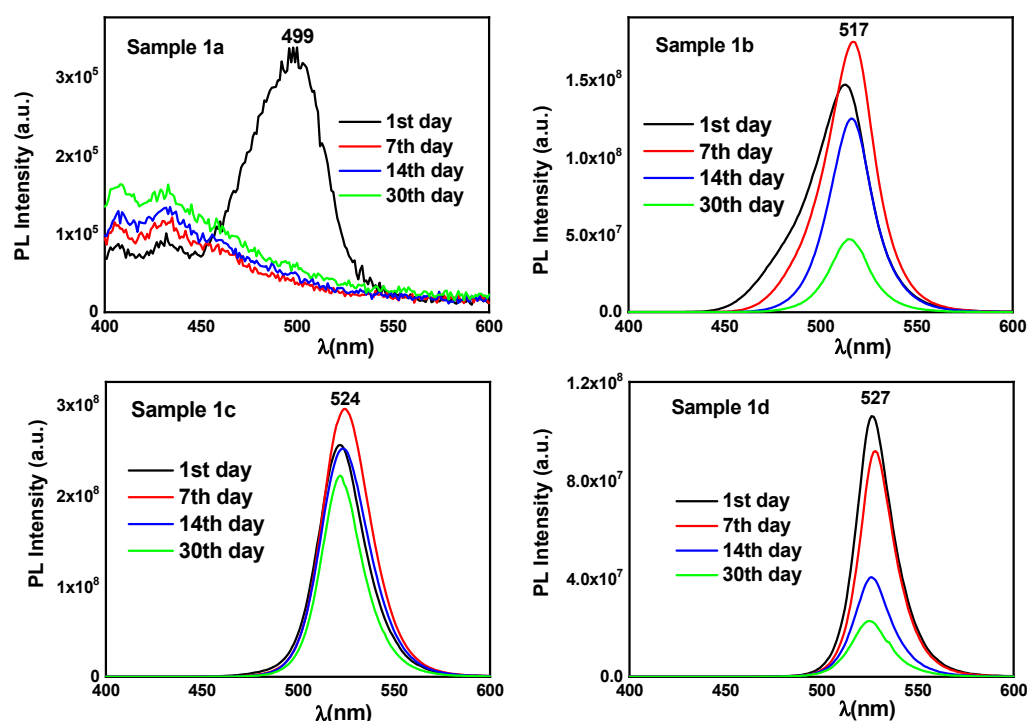

Figure 4. Fluorescence emission spectra of solutions (1a), (1b), (1c), and (1d) from 1st (black line), 7th (red line), 14th (blue line), and 30th (green line) day.

To the analogues blank solutions without the polymer addition, precipitation observed after some hours. Consequently, no absorption peaks and very weak fluorescence peaks were observed (see Figure S3). Decrease of the absorption and emission values, as time passes, comprise an indication that the colloidal stability of perovskite/polymer hybrid system is decreased. The decrease of the colloidal stability is also confirmed by the dynamic light scattering results, where the value of the hydrodynamic radius is also increased. On the other hand, for the samples of series 2, precipitation occurs after some hours and do not exhibit excitonic absorption or PL emission, indicating that no stable nanocrystals were rated in the absence of copolymer (see Figure S4).

3.2.2. Time-Resolved Photoluminescence Decay Studies

In order to study further the photoluminescence properties of the perovskite/polymer hybrid solutions, photoluminescence decay studies were performed and compared with those of the perovskite solution without the presence of the random copolymer dispersed in toluene (blank experiment).

Firstly, fresh solutions of Samples 1d and 2d were prepared and the fluorescence lifetime profiles for both perovskite/polymer hybrid system and free perovskite dispersed in toluene were obtained immediately and analyzed (Figure 5). The analysis of the time profile of the fluorescence decay at 375 nm for the free perovskite dispersed in toluene showed only one component with 1.14 ns lifetime, while two components were detected for the perovskite/polymer hybrid material; a faster one with 90 ps lifetime (18%), assigned to perovskite nanocrystals, which probably were not encapsulated into the polymer containing nanoparticles, and a slower one in a much higher percentage (82%) with 9.8 ns lifetime, attributed to the hybrid nanomaterial. These values are significantly lower than those of bulk films (~100 ns) [40,41]. A possible scenario is that the short (90 ps) lifetime corresponds to a low ratio (18%) of perovskite nanocrystals, which probably were not encapsulated into the polymer containing nanoparticles, and thus they are not colloidal stable and exhibit short lifetime properties. The longer lifetime in a much higher percentage (82%) with 9.8 ns lifetime is assigned to the hybrid nanomaterial possibly due to a reduction of the defect density that the incorporation of the polymer matrix established. The polymer matrix probably decreases the defect sites and removes trapped states, a fact that leads to the elongation of photoluminescence decay time [42].
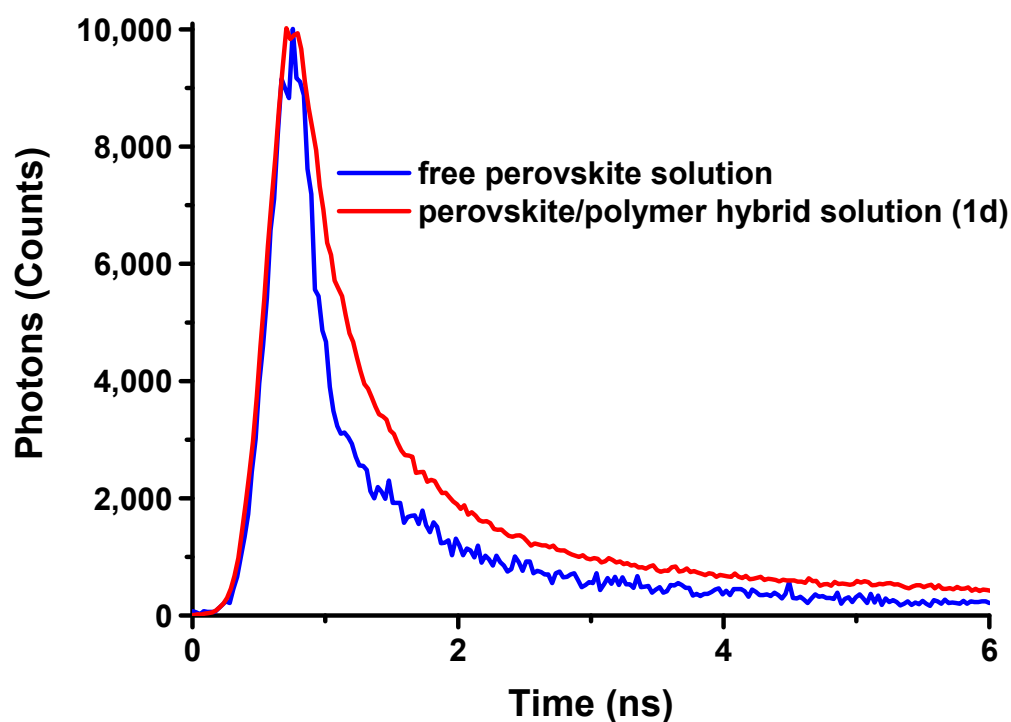

Figure 5. Lifetime decays of perovskite solution of C = 50.08 mM dispersed in toluene, without the presence of the random copolymer, (blue line) and Sample 1d (red line).

As a result, photoluminescence decay assays reinforce the belief that the PMMA-co- PDMAEMA random copolymer functions as a protective matrix against perovskite precipitation and also provides colloidal and temporal stability.

3.2.3. Perovskite/Polymer Hybrid Thin-Films

Furthermore, we investigate the photoluminescence intensity of perovskite/polymer thin films (Samples TFa, TFb, TFc, TFd), which were prepared by homogenous coating of Samples 1a, 1b, 1c, 1d on a glass surface, respectively. The aim of this experiment is to investigate if the copolymer/perovskite hybrid system is capable of exhibiting emissions in absence of toluene and therefore could be applied as active components of an OLED device. UV-Vis absorption and fluorescence emission were studied at regular time intervals

in order to determine time stability of the thin-films optical/photophysical properties. The results are presented in Table 3.

Table 3. Thin-Film samples, their precursor solutions, thickness of the films, and concentration of perovskite in each sample.

Precursor Solution	Thin-Film Sample Code	C Perovskite in DMF (mM)	Thickness (μm)
1a	TFa	6.26	1500.3
1b	TFb	12.52	4900.4
1c	TFc	25.04	1700.8
1d	TFd	50.08	3400.2

A redshift is observed in both absorbance and emission spectra when the concentration of the perovskite in the film is increased due to the increase of the nanocrystals size (Figures 6 and 7). In the case of sample TFa, the UV-Vis absorption spectrum exhibits an excitonic peak at λ = 505 nm, and an emission peak at 510 nm, both peaks disappeared at the second measurement (11th day). The same behavior was observed for the TFb sample, but although the excitonic absorption at ~516 nm has disappeared, on the 11th day there was still a significant emission signal (Figures 6 and 7). The characteristic peaks due to exciton appear at the fresh films of the hybrid samples TFa, TFb, TFc, and TFd (Figures 6 and 8).
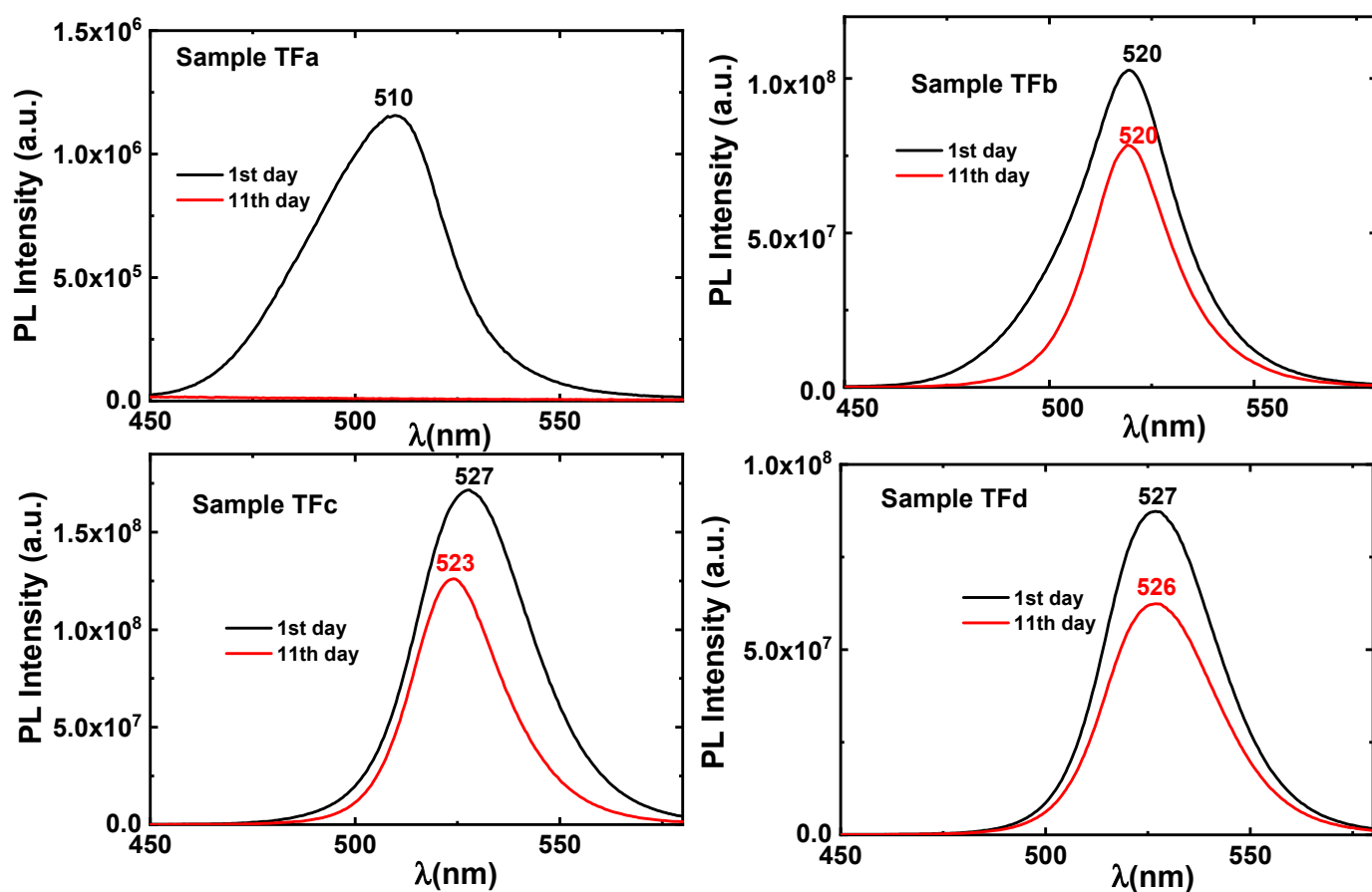

Figure 6. Fluorescence emission spectra of thin-films (TFa), (TFb), (TFc), (TFd) on day 1 (black line) and day 11 (red line).
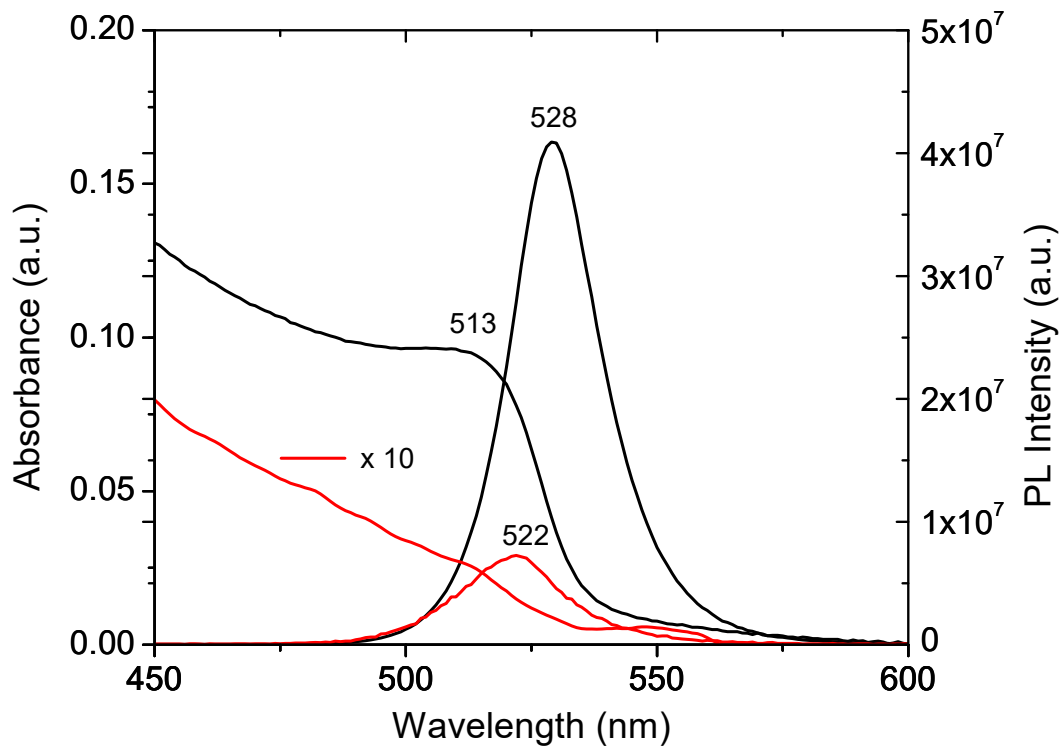
Figure 7. UV-Vis absorption and fluorescence emission spectra of TFc (red line) and TFd (black line), after 2 months.
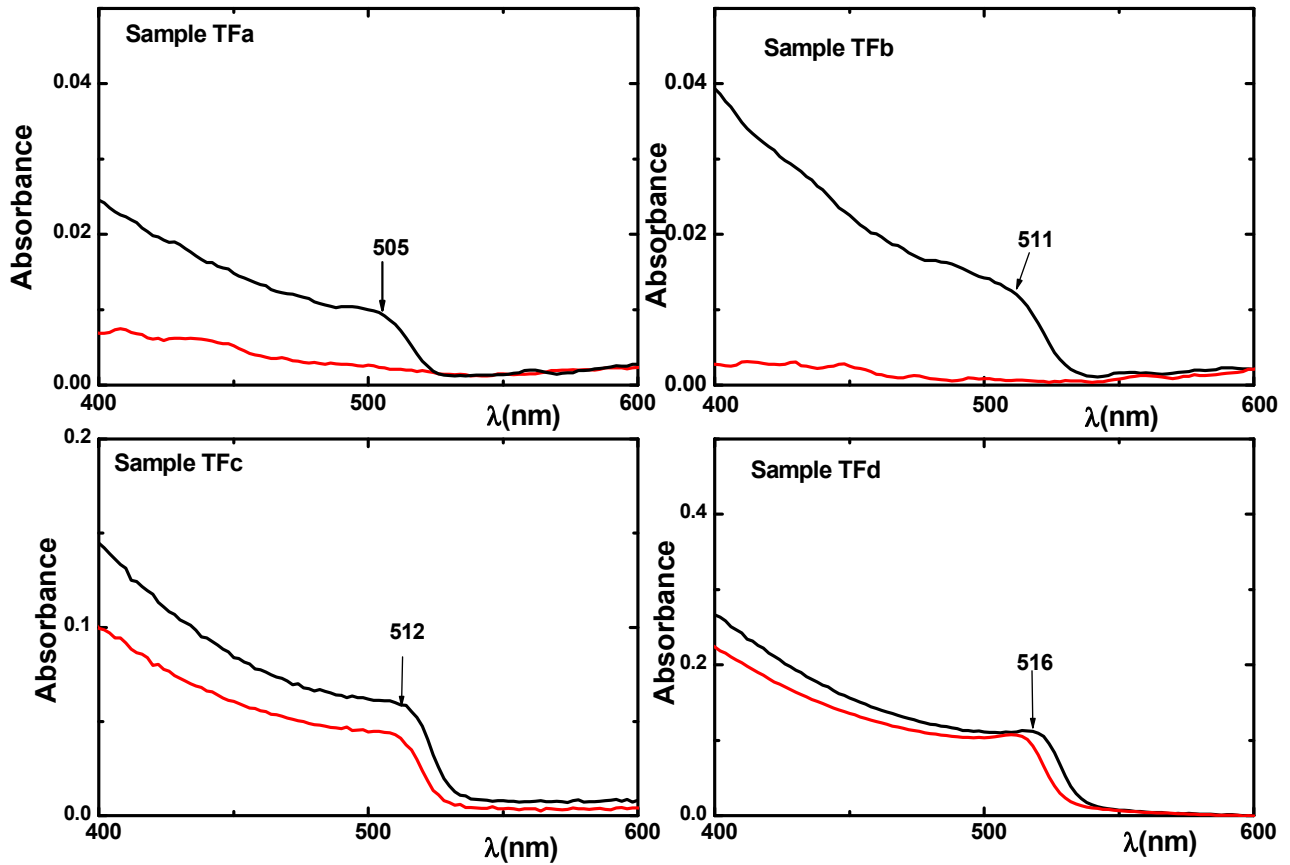

Figure 8. UV-Vis absorption spectra of thin- films (TFa), (TFb), (TFc), and (TFd) on day 1 (black line) and day 11 (red line).

In the case of sample TFa, the UV-Vis absorption spectrum exhibits an excitonic peak at λ = 505 nm and an emission peak at 510 nm, both peaks disappeared at the second measurement (11th day). The same behavior was observed for the TFb sample, but although the excitonic absorption at ~516 nm disappeared, on the 11th day there was still a significant emission signal (Figures 6 and 8). The excitonic peaks of the samples TFc and TFd in both, absorbance and emission spectra, remain strong even after two years (Figure 7 and Figure S6) and can be observed even with naked eye, indicating a strong stability in the matrix.

4. Conclusions

Perovskite ($CH_3NH_3PbBr_3$)/P(MMA-co-DMAEMA) random copolymer hybrid nanomaterials were successfully prepared using toluene as the solvent where the hybrid nanoparticles were dispersed. The self-organization of the P(MMA-co-DMAEMA) random copolymer in toluene results in the formation of nanoaggregates where the DMAEMA segments make up the nanoparticle core and the MMA units the corona. Addition of the perovskite-DMF solution into the colloidal solution of the random copolymer, ends up in the encapsulation of the perovskite nanocrystal into the DMAEMA domains, while MMA parts function as the provider of colloidal stability to the hybrid nanosystem. Size and size polydispersity of the nanoparticles were determined by dynamic light scattering experiments. The solutions showed increased stability for more than a month in some cases. Thin-films prepared via spin-coating of the perovskite/polymer solutions, exhibit great similarity in the optical characteristics with the precursor solutions. They are capable of emitting light for long time periods (up to two years). As a result, perovskite ($CH_3NH_3PbBr_3$)/P(MMA-co-DMAEMA) random copolymer hybrid system constitutes a new emerging class of hybrid materials, exhibiting great optical properties and they could be utilized in the development of photovoltaic devices.

Supplementary Materials: The following are available online at https://www.mdpi.com/article/10.3390/jcs5110304/s1, Figure S1: ^{1}H-NMR spectrum of the P(MMA-co-DMAEMA) random copolymer, Figure S2: ATR-FTIR spectrum of the P(MMA-co-DMAEMA) random copolymer, Figure S3: UV-Vis absorption spectra of solutions 2a, 2b, 2c and 2d from 1st (black line), 7th (red line) 14th (Blue line) and 30th (green line) day, Figure S4: Fluorescence emission spectra of solutions 2a, 2b, 2c and 2d from 1st (black line), 7th (red line) 14th (Blue line) and 30th (green line) day, Figure S5: Comparative ATR-FTIR spectra of the hybrid material (red line) and polymer matrix (black line), Figure S6: Photo of solutions 1a, 1b, 1c and 1d under UV light, on the day they were prepared, Figure S7: TEM images from sample 1b (a) and (b), sample 1c (c) and (d).

Author Contributions: S.P., G.M. and M.K., designed the experiments; M.K. conducted the experiments; S.P. and G.M. contributed the materials/reagents and instrumentation and supervised the project; M.K., G.M. and S.P. analyzed the experimental data and wrote the manuscript. All authors have read and agreed to the published version of the manuscript.

Conflicts of Interest: The authors declare no conflict of interest.

References

1.   Mousdis, G.A.; Papavassiliou, G.C.; Raptopoulou, C.P.; Terzis, A. Preparation and characterization of [$H_3N(CH_2)_6NH_3$]PbI_4 and similar compounds with a layered perovskite structure. *J. Mater. Chem.* **2000**, *10*, 515–518. [CrossRef]

2. Papavassiliou, G.C.; Mousdis, G.A.; Koutselas, I. Basic Properties and Early Works in Organic–Inorganic Perovskites. In *Halide Perovskites: Photovoltaics, Light Emitting Devices, and Beyond*; Sum, T.-C., Mathews, N., Eds.; Wiley-VCH GmbH & Co.: Hoboken, NJ, USA, 2019.

3. Stoumpos, C.C.; Malliakas, C.D.; Kanatzidis, M.G. Semiconducting tin and lead iodide perovskites with organic cations: Phase transitions, high mobilities, and near-infrared photoluminescent properties. *Inorg. Chem.* **2013**, *52*, 9019–9038. [CrossRef]

4. Xing, G.; Mathews, N.; Sun, S.; Lim, S.S.; Lam, Y.M.; Grätzel, M.; Mhaisalkar, S.; Sum, T.C. Long-range balanced electron- and hole-transport lengths in organic–inorganic $CH_3NH_3PbI_3$. *Science* **2013**, *342*, 344–347. [CrossRef]

5. Stranks, S.D.; Eperon, G.E.; Grancini, G.; Menelaou, C.; Alcocer, J.P.M.; Leijtens, T.; Herz, M.L.; Petrozza, A.; Snaith, H.J. Electron–hole diffusion lengths exceeding 1 micrometer in an organometal trihalide perovskite absorber. *Science* **2013**, *342*, 341–344. [CrossRef]

6. Papavassiliou, G.C.; Vidali, M.S.; Pagona, G.; Mousdis, G.A.; Karousis, N.; Koutselas, I. Effects of organic moieties on the photoluminescence spectra of perovskite-type tin bromide based compounds. *J. Phys. Chem. Solids* **2015**, *79*, 1–6. [CrossRef]

7. Papavassiliou, G.C.; Mousdis, G.A.; Pagona, G.; Karousis, N.; Vidali, M.S. Room temperature enhanced blue-green, yellow-orange and red phosphorescence from some compounds of the type $(CH_3NH_3)_{n-1}$(1-naphthylmethyl ammonium)$_2Pb_n(Cl_xBr_{1-x})_{3n+1}$ (with n = 1, 2 and $0 \leq x \leq 1$) and related observations from similar compounds. *J. Lumin.* **2014**, *149*, 287–291. [CrossRef]

8. Papavassiliou, G.C.; Mousdis, G.A.; Koutselas, I. Excitonic bands in the spectra of some organic-inorganic hybrid compounds based on metal halide units. *Mon. Chem.* **2001**, *132*, 113–119. [CrossRef]

9. Papavassiliou, G.C.; Mousdis, G.A.; Anyfantis, G.C.Z. Organic-inorganic hybrid compounds based on lead halide units: Preparation from melts and through grinding effects. *Z. Nat. B* **2010**, *65*, 516–520. [CrossRef]

10. Eperon, G.E.; Stranks, S.D.; Menelaou, C.; Johnston, M.B.; Herz, L.M.; Snaith, H.J. Formamidinium lead trihalide: A broadly tunable perovskite for efficient planar heterojunction solar cells. *Energy Environ. Sci.* **2014**, *7*, 982–988. [CrossRef]

11. Zhang, F.; Zhong, H.; Chen, C.; Wu, X.G.; Hu, X.; Huang, H.; Han, J.; Zou, B.; Dong, Y. Brightly luminescent and color-tunable colloidal CH3NH3PbX3 (X = Br, I, Cl) quantum dots: Potential alternatives for display technology. *ACS Nano* **2015**, *9*, 4533–4542. [CrossRef]

12. Zhao, Y.; Zhu, K. Organic–inorganic hybrid lead halide perovskites for optoelectronic and electronic applications. *Chem. Soc. Rev.* **2016**, *45*, 655–689. [CrossRef]

13. Tan, Z.-K.; Moghaddam, R.S.; Lai, M.L.; Docampo, P.; Higler, R.; Deschler, F.; Price, M.; Sadhanala, A.; Pazos, L.M.; Credgington, D.; et al. Bright light-emitting diodes based on organometal halide perovskite. *Nat. Nanotechnol.* **2014**, *9*, 687–692. [CrossRef]

14. Fang, Y.; Dong, Q.; Shao, Y.; Yuan, Y.; Huang, J. Highly narrowband perovskite single-crystal photodetectors enabled by surface-charge recombination. *Nat. Photonics* **2015**, *9*, 679–686. [CrossRef]

15. Zhu, H.; Fu, Y.; Meng, F.; Wu, X.; Gong, Z.; Ding, Q.; Gustafsson, M.V.; Trinh, M.T.; Jin, S.; Zhu, X.Y. Lead halide perovskite nanowire lasers with low lasing thresholds and high quality factors. *Nat. Mater.* **2015**, *14*, 636–642. [CrossRef]

16. Mei, Y.; Zhang, C.; Vardeny, Z.; Jurchescu, O. Electrostatic gating of hybrid halide perovskite field-effect transistors: Balanced ambipolar transport at room-temperature. *MRS Commun.* **2015**, *5*, 297–301. [CrossRef]

17. Yang, S.; Fu, W.; Zhang, Z.; Chen, H.; Li, C.Z. Recent advances in perovskite solar cells: Efficiency, stability and lead-free perovskite. *J. Mater. Chem. A* **2017**, *5*, 11462–11482. [CrossRef]

18. Veldhuis, S.A.; Boix, P.P.; Yantara, N.; Li, M.; Sum, T.C.; Mathews, N.; Mhaisalkar, S.G. Perovskite Materials for Light-Emitting Diodes and Lasers. *Adv. Mater.* **2016**, *28*, 6804–6834. [CrossRef]

19. Uchman, M.; Procházka, K.; Gatsouli, K.; Pispas, S.; Špírková, M. CdS-containing nano-assemblies of double hydrophilic block copolymers in water. *Colloid Polym. Sci.* **2011**, *289*, 1045–1053. [CrossRef]

20. Móller-Buschbaum, P.; Thelakkat, M.; Fassler, F.T.; Stutzmann, M. Hybrid Photovoltaics—From Fundamentals towards Application. *Adv. Energy Mater.* **2017**, *7*, 1700248. [CrossRef]

21. Huang, H.; Bodnarchuk, M.; Kershaw, S.; Kovalenko, M.; Rogach, A. Lead Halide Perovskite Nanocrystals in the Research Spotlight: Stability and Defect Tolerance. *ACS Energy Lett.* **2017**, *9*, 2071–2083. [CrossRef]

22. Sichert, J.A.; Tong, Y.; Mutz, N.; Vollmer, M.; Fischer, S.; Milowska, K.Z.; García Cortadella, R.; Nickel, B.; Cardenas-Daw, C.; Stolarczyk, J.K.; et al. Quantum size effect in organometal halide perovskite nanoplatelets. *Nano Lett.* **2015**, *15*, 6521–6527. [CrossRef] [PubMed]

23. Schmidt, L.C.; Pertegas, A.; Gonzalez-Carrero, S.; Malinkiewicz, O.; Agouram, S.G.; Minguez Espallargas, G.; Bolink, H.J.; Galian, R.E.; Perez-Prieto, J. Nontemplate Synthesis of $CH_3NH_3PbBr_3$ Perovskite Nanoparticles. *J. Am. Chem. Soc.* **2014**, *136*, 850–853. [CrossRef]

24. Gonzalez-Carrero, S.; Galian, R.E.; Perez-Prieto, J. Maximizing the emissive properties of $CH_3NH_3PbBr_3$ perovskite nanoparticles. *J. Mater. Chem. A* **2015**, *3*, 9187–9193. [CrossRef]

25. Papavassiliou, G.C.; Pagona, G.; Mousdis, G.A.; Karousis, N. Enhanced phosphorescence from nanocrystalline/microcrystalline materials based on (CH_3NH_3)(1-naphthylmethyl ammonium)$_2Pb_2Cl7$ and similar compounds. *Chem. Phys. Lett.* **2013**, *570*, 80–84. [CrossRef]

26. Protesescu, L.; Yakunin, S.; Bodnarchuk, M.I.; Krieg, F.; Caputo, R.; Hendon, C.H.; Yang, R.X.; Walsh, A.; Kovalenko, M.V. Nanocrystals of cesium lead halide perovskites (CsPbX3, X = Cl, Br, and I): Novel optoelectronic materials showing bright emission with wide color gamut. *Nano Lett.* **2015**, *15*, 3692–3696. [CrossRef]

27. Förster, S.; Antonietti, M. Amphiphilic block copolymers in structure-controlled nanomaterial hybrids. *Adv. Mater.* **1998**, *10*, 195–217. [CrossRef]

28. Mai, Y.; Eisenberg, A. Self-assembly of block copolymers. *Chem. Soc. Rev.* **2012**, *41*, 5969–5985. [CrossRef] [PubMed]

29. Kaditi, H.; Mountrichas, G.; Pispas, S. Amphiphilic block copolymers by a combination and selective post-polymerization functionalization. *Eur. Polym. J.* **2011**, 415–434. [CrossRef]

30. Kafetzi, M.; Pispas, S. Multifaceted pH and Temperature Induced Self-Assembly of P(DMAEMA-co-LMA)-b-POEGMA Terpolymers and Their Cationic Analogues in Aqueous Media. *Macromol. Chem. Phys.* **2021**, *222*, 2000358. [CrossRef]

31. Mountrichas, G.; Pispas, S.; Kamitsos, E. Effect of Temperature on the Direct Synthesis of Gold Nanoparticles Mediated by Poly(dimethylaminoethyl methacrylate) Homopolymer. *J. Phys. Chem. C* **2014**, *118*, 22754–22759. [CrossRef]

32. Gao, M.; Yu, S.; Yuan, J.; Zhang, W.; Antonietti, M. Poly(ionic liquid)-Mediated Morphogenesis of Bismuth Sulfide with a Tunable Band Gap and Enhanced Electrocatalytic Properties. *Angew. Chem. Int. Ed.* **2016**, *55*, 12812–12816. [CrossRef]

33. Vlassi, E.; Mousdis, G.A.; Pispas, S. Nickel dithiolene complexes encapsulated in biocompatible amphiphilic diblock copolymer nanoparticles. *J. Pol. Sci. Part. B Pol. Phys.* **2016**, *54*, 2507–2513. [CrossRef]

34. Michman, E.; Shenhar, R. Directed self-assembly of block copolymer based nanocomposites in thin films. *Polym. Adv. Technol.* **2017**, *28*, 613–622. [CrossRef]

35. Des Cloizeaux, J.; Jannink, G. *Polymers in Solution Their Modelling and Structure*; Clarendon Press: Oxford, UK, 1990; Chapter 10; pp. 415–417.

36. Provencher, S. CONTIN: A general purpose constrained regularization program for inverting noisy linear algebraic and integral equations. *Comp. Phys. Commun.* **1982**, *27*, 229–242. [CrossRef]

37. Zhang, Z.Y.; Wang, H.Y.; Zhang, Y.X.; Hao, Y.W.; Sun, C.; Zhang, Y.; Gao, B.R.; Chen, Q.D.; Sun, H.B. The Role of Trap-assisted Recombination in Luminescent Properties of Organometal Halide $CH_3NH_3PbBr_3$ Perovskite Films and Quantum Dots. *Sci. Rep.* **2016**, *6*, 27286. [CrossRef] [PubMed]

38. Shi, D.; Adinolfi, V.; Comin, R.; Yuan, M.; Alarousu, E.; Buin, A.; Chen, Y.; Hoogland, S.; Rothenberger, A.; Katsiev, K.; et al. Low Trap-State Density and Long Carrier Diffusion in Organolead Trihalide Perovskite Single Crystals. *Science* **2015**, *347*, 519–522. [CrossRef]

39. Kojima, A.; Ikegami, M.; Teshima, K.; Miyasaka, T. Highly Luminescent Lead Bromide Perovskite Nanoparticles Synthesized with Porous Alumina Media. *Chem. Lett.* **2012**, *41*, 397–399. [CrossRef]

40. Zhang, M.; Yu, H.; Lyu, M.; Wang, Q.; Yun, J.H.; Wang, L.Z. Composition-dependent photoluminescence intensity and prolonged recombination lifetime of perovskite $CH_3NH_3PbBr_{3-x}Cl_x$ films. *Chem. Commun.* **2014**, *50*, 11727–11730. [CrossRef]

41. Du, J.S.; Shin, D.; Stanev, R.K.; Musumeci, C.; Xie, Z.; Huang, Z.; Lai, M.; Sun, L.; Zhou, W.; Stern, N.P.; et al. Halide perovskite nanocrystals arrays: Multiplexed synthesis and sizedependent emission. *Sci. Adv.* **2020**, *6*, eabc4959. [CrossRef] [PubMed]

42. Zuo, L.; Guo, H.; de Quilettes, D.W.; Jariwala, S.; De Marco, N.; Dong, S.; DeBlock, R.; Ginger, D.S.; Dunn, B.; Wang, M.; et al. Polymer-modified halide perovskite films for efficient and stable planar heterojunction solar cells. *Sci. Adv.* **2017**, *3*, e1700106. [CrossRef]